Controlling intramolecular and intermolecular electronic coupling of radical ligands in a series of cobaltoviologen complexes

Brice J. O. Kessler, Iram F. Mansoor, Derek I. Wozniak, Thomas J. Emge, and Mark C. Lipke*

Department of Chemistry and Chemical Biology, Rutgers, The State University of New Jersey, 123 Bevier Road, Piscataway, New Jersey 08854, United States

ABSTRACT: Controlling electronic coupling between two or more redox sites is of interest for tuning the electronic properties of molecules and materials. While classic mixed-valence (MV) systems are highly tunable, e.g., via the modular organic bridges connecting the redox sites, metal-bridged MV systems are difficult to control because the electronics of the metal cannot usually be altered independently of redox-active moieties embedded in its ligands. Herein, we overcome this limitation by varying the donor strengths of ancillary ligands in a series of cobalt complexes without directly perturbing the electronics of viologen-like redox sites bridged by the cobalt ions. The cobaltoviologens **[1$_X$-Co]$^{n+}$** feature four 4-X-pyridyl donor groups (X = CO_2Me, Cl, H, Me, OMe, NMe_2) that provide gradual tuning of the electronics of the bridging Co^{II} centers, while a related complex **[2-Co]$^{n+}$** with NHC donors supports exclusively Co^{III} states even upon reduction of the viologen ligands. Electrochemistry and IVCT band analysis reveal that the MV states of these complexes have electronic structures ranging from fully localized (**[2-Co]$^{4+}$**; Robin-Day Class I) to fully delocalized (**[1$_{CO2Me}$-Co]$^{3+}$**; Class III) descriptions, demonstrating unprecedented control over electronic coupling without changing the identity of the redox sites or bridging metal. Additionally, single-crystal XRD characterization of the homovalent complexes **[1$_H$-Co]$^{2+}$** and **[1$_H$-Zn]$^{2+}$** revealed radical-pairing interactions between the viologen ligands of adjacent complexes, representing a type of through-space electronic coupling commonly observed for organic viologen radicals but never before seen in metalloviologens. The extended solid-state packing of these complexes produces 3D networks of radical π-stacking interactions that impart unexpected mechanical flexibility to these crystals.

Introduction.

Mixed-valence (MV) systems that show electronic coupling between their redox sites are of longstanding interest[1,2] for their nuanced electronic structures,[3] which lie on a continuum from fully localized[2a,b] to fully delocalized[2f,g] descriptions (Scheme 1A), as well as for the influence that these features have on electron transfer in contexts ranging from solar-energy harvesting[4] to conductive materials.[5] Delocalization can also influence other chemical and physical properties of MV systems,[6] further motivating interest in controlling electronic coupling between redox sites. Classic MV examples, possessing two redox-active metal sites connected by a π-conjugated bridge (Scheme 1B),[2e] have been tuned by changing the metal centers,[7] the bridge,[8] or the ancillary ligands.[9] Likewise, organic MV systems have proven to be exceptionally tunable owing to the synthetic versatility of organic chemistry.[10-12] These examples reveal how coupling is influenced by a variety of factors, including the length and conjugation pathway of the bridge,[11] as well as its orbital energies relative to those of the redox sites.[10b,12] However, there remain substantial limitations to the control that can be attained over electronic delocalization in many MV systems, especially those in which two organic redox sites are coupled by a bridging metal ion.[13]

Though less studied than bimetallic and fully organic examples, metal-bridged MV systems include complexes of redox-active salen,[2g,14] diarylamido,[15] pyridine-diimine (PDI),[16] and dithiolene ligands (Scheme 2A).[17,18] In all these

Scheme 1. Electronically coupled redox systems.

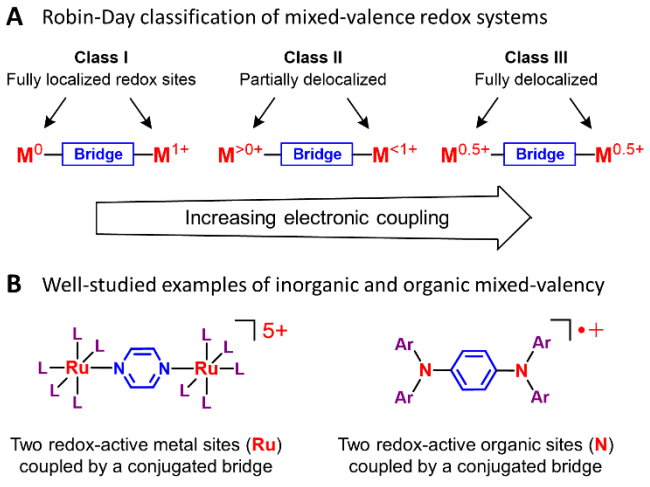

complexes, the ligand-based redox activity heavily involves donor atoms bound to the bridging metal,[19] making it challenging to independently tune the properties of the redox sites and the bridge. Thus, while reduction potentials of such complexes can be altered by >500 mV using electron-donating (ED) and -withdrawing (EW) substituents, these changes weakly influence electronic coupling of the ligands.[14a,b,15b,16a] A series of aluminum bis-PDI complexes was recently shown to exhibit reduction potentials spanning a

Scheme 2. Tuning Metal-Mediated Electronic Coupling of Organic Redox Sites

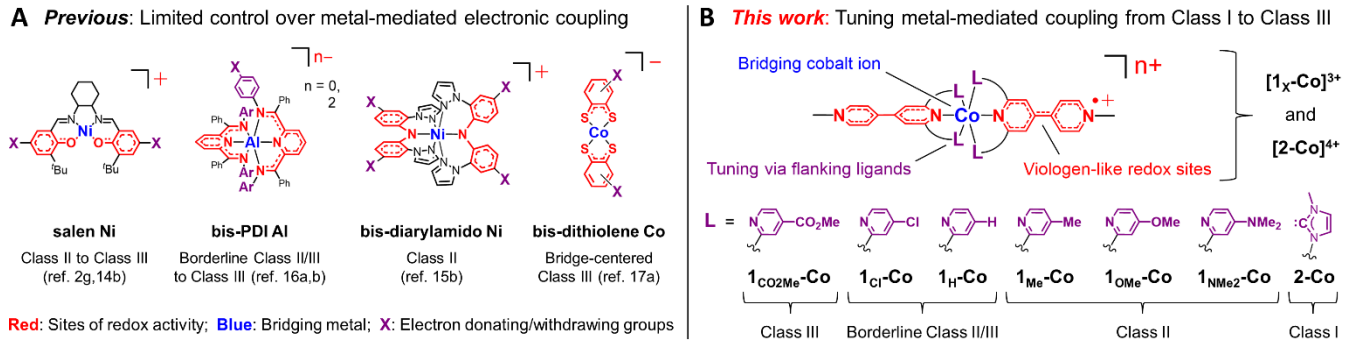

0.5 V range while maintaining Robin-Day Class III (fully delocalized) or borderline Class II/III (nearly fully delocalized) descriptions.[16a] Greater variation in coupling, from Class II (moderately coupled) to Class III descriptions, was seen in a series of substituted nickel-salen complexes, but required a 0.77 V variation in the reduction potentials of the ligands.[14a,b] On the other extreme, changing the identity of the bridging metal often disrupts delocalization considerably,[6a,13c,15a] providing only a crude tool for tuning such systems. Identifying more-precisely tunable metal-bridged MV systems would fill an important gap in the study of mixed valency, and may also lead to practical advances considering that certain delocalized complexes (e.g., cobalt bis-dithiolenes) are useful for assembling functional conductive materials (e.g., conductive[5d,e] and electrocatalytic[20] MOFs).

We recently discovered that cobalt mediates borderline Class II/III electronic coupling between viologen-like redox sites embedded in simple terpyridine ligand scaffolds (complex **[1H-Co]3+** in Scheme 2B).[6a] Since redox-activity is centered almost entirely on the viologen cores, we hypothesized that the flanking donor groups of the ligand could be altered to modulate the electronics of the cobalt bridge without directly perturbing the organic redox sites (Scheme 2B), thereby affording substantial control over the ability of cobalt to mediate coupling between these sites. Herein, we describe the success of this strategy at gradually tuning the MV states of the cobaltoviologens from Class I to Class III descriptions, representing a range of variation and degree of control unavailable in any other series of metal-bridged MV systems that maintain a fixed set of redox sites and bridging metal.

We also discovered that the more-reduced complex **[1H-Co]2+** and its zinc analogue **[1H-Zn]2+** can engage in intermolecular radical-pairing interactions that are characteristic of organic viologens,[21] but which have not been observed before in metalloviologens. Such interactions contribute to the conductivity of viologen-radical crystals and have been utilized to prepare (supra)molecular structures with unique electronic and mechanical properties.[22] Thus, the ability of metalloviologens to participate in similar interactions is a notable finding that suggests these complexes may provide a rich basis for developing new materials. Indeed, **[1H-Co]2+** and **[1H-Zn]2+** pack into 3D networks of radical π-stacking interactions, with the specific packing motif influenced by metal-ligand electronic interactions, but in both cases giving rise to crystals with emergent mechanical flexibility that is not observed in organic viologen crystals.

Results and Discussion.

Design and synthesis of new cobaltoviologens. The complex **[1H-Co]4+** was first reported over 20 years ago,[23] but it was only recently discovered that its reduced state **[1H-Co]3+** exhibits a delocalized electronic structure, in contrast to the corresponding Fe^{II}, Ni^{II}, and Zn^{II} complexes, which all undergo localized reductions of their ligands.[6a,24] A half-filled 3d orbital of d_{xz}/d_{yz} parentage appears to be important for the delocalized electronic structure of the cobalt derivative,[6a] so tuning the energy and occupancy of this orbital was targeted to control its ability to facilitate inter-ligand electronic coupling. The Co^{II}/Co^{I} reduction potentials of simple $[(terpy)_2Co]^{2+}$ complexes can be modified across a wide range using electron donating or withdrawing substituents on the flanking pyridyl groups,[25] suggesting an easy approach to tune the electronics of the cobalt bridge in **[1x-Co]n+**. Additionally, it was envisioned that strong donor groups might even lead to changes of the spin state or oxidation state of the cobalt center, which would offer a novel way to control electronic coupling between the ligands in these complexes.

A series of new terpy-viologen ligands **1x+** was prepared with 4-position substituents (X = CO_2Me, Cl, Me, OMe, NMe_2) on the flanking pyridyl groups that provide a well-spaced gradient from strongly electron withdrawing to strongly electron donating (Scheme 3). In all cases, the new ligands were prepared from 4-substituted-2-acetylpyridines using the established terpyridine synthesis and *N*-methylation sequence used to prepare unsubstituted **1H+** (see SI for full synthetic details).[26,27] Once the ligands **1x+** were isolated as their chloride salts, they readily formed the bis-terpy complexes **[1x-Co]4+** and **[1x-Zn]4+** upon treatment with $CoCl_2•6H_2O$ or $Zn(OAc)_2•2H_2O$, respectively. Paramagnetic ^1H NMR spectra (Figures S19-S23) and UV-vis spectra

Scheme 3. Synthesis of [1x-Co]•nPF6 and [1x-Zn]•4PF6.

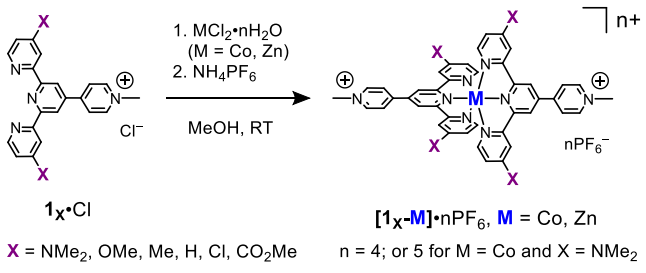

(Figures S70, S74, S78, S82, S87) of the cobalt series suggest that most of these complexes have similar electronic structures in which a high-spin Co^{II} state predominates. However, the dimethylamino-substituted derivative was found to oxidize to a Co^{III} state under air, so samples were isolated in this higher oxidation state (**[1$_{NMe2}$-Co]$^{5+}$**) for ease of handling (see Figure S22 for diamagnetic ^{1}H NMR spectrum).

The reduced complex **[1$_{NMe2}$-Co]$^{3+}$** shows the weakest inter-ligand electronic coupling of the MV **[1$_X$-Co]$^{3+}$** series of complexes, but still maintains Class II coupling (vide infra). To access more dramatic electronic changes in the cobaltoviologens, a bis-NHC-viologen pincer ligand **2$^+$** was designed to provide more strongly donating flanking groups. The NHC ligand precursor **2-H^{3+}** was prepared readily (Scheme 4) by nucleophilic aromatic substitution of 2,6-dichloro-4,4'-bipyridine with *N*-methylimidazole, followed by methylation of the 4-pyridyl group. Metallation of **2-H^{3+}** with cobalt was achieved by deprotonating the ligand precursor with LiHMDS at −100 °C in THF, followed by treatment with $CoCl_2$, and lastly, oxidation with $AgPF_6$ to provide the Co^{III} complex [**2-Co]$^{5+}$** (Scheme 4). Though less straightforward than preparation of the **[1$_X$-Co]$^{n+}$** complexes, [**2-Co]$^{5+}$** was successfully isolated and characterized by ^{1}H NMR spectroscopy and ESI-HRMS (Figures S38, S39, S51).

Scheme 4. Synthesis of [2-Co]•5PF$_6$.

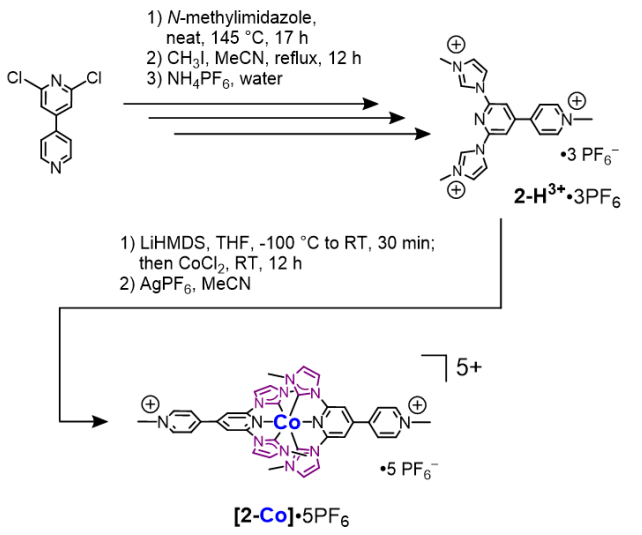

Electrochemical characterization. Cyclic voltammetry was used to examine the redox properties of the new metalloviologens, revealing how the flanking donor groups affect the reduction potentials of the viologen units and the extent to which these redox processes are influenced by inter-ligand electronic coupling. None of the zinc complexes show separation of the first reductions of each ligand (Figures 1 and S61 – S66), consistent with a lack of electronic communication through the Zn^{II} bridge. The $E_{1/2}$ values (−0.95 to −1.12 V vs. $Fc^{+/0}$) for these ligand-centered 2 e$^-$ redox processes vary with the electron-donating/withdrawing character of the substituents on the ligands, showing a good linear correlation with their σ_p Hammet parameters but not with the corresponding σ_m values (Figure S67). Since the substituents on the flanking groups are in the *meta* position relative to the viologen moieties, the correlation of $E_{1/2}$ with σ_p but not σ_m suggests that the flanking pyridyl groups influence the redox properties of the viologens by tuning the Lewis acidity of the Zn^{II} ion rather than via direct inductive effects. Two closely overlapping 1 e$^-$ reductions follow the 2 e$^-$ first reduction, and the consistently small spacing (68 – 81 mv) between these 1 e$^-$ reductions confirms the absence of significant electronic communication between the ligands in any of the redox states of **[1$_X$-Zn]$^{n+}$**.

The **[1$_X$-Co]$^{n+}$** series exhibits redox behavior differing significantly from that of their zinc counterparts. The cobalt complexes all show four distinct 1 e$^-$ redox couples involving the viologen units (Figure 1 and Table 1), with the separation between the first and second of these reductions changing from $\Delta E_{red1,2}$ = 122 mV to $\Delta E_{red1,2}$ = 396 mV ($\Delta\Delta E_{red1,2}$ = 274 mV) across the series from **[1$_{NMe2}$-Co]$^{n+}$** to **[1$_{CO2Me}$-Co]$^{n+}$**. The increasing separation corresponds to increasing electronic coupling between the ligands in the 3+ state,[28] confirming that the flanking donor groups are effective for tuning delocalization across the L-Co-L core. Interestingly, the midpoint between the first and second reductions, which approximates what the potential of the ligand-centered reduction would be in the absence of coupling, changes by only 237 mV across this series (see Table 1). This observation confirms that the electronics of the **1$_X$-Co** complexes are influenced more by variation in electronic coupling between the ligands than by variation of the

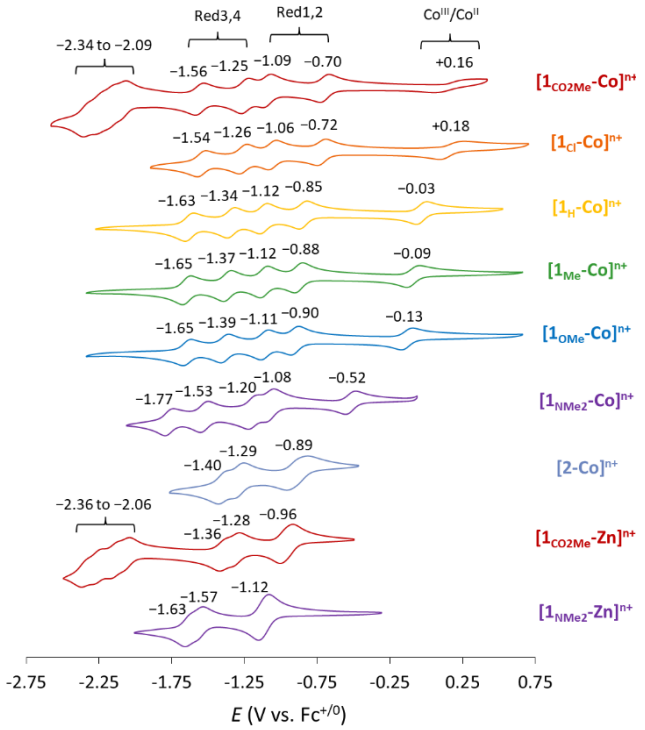

Figure 1. Cyclic voltammograms of **[1$_X$-Co]**$(PF_6)_n$, **[2-Co]**$(PF_6)_5$, and select **[1$_X$-Zn]**$(PF_6)_4$ complexes in MeCN containing 0.1 M $TBAPF_6$. The $E_{1/2}$ values of each redox couple are indicated to the nearest 10 mV, except for reductions of the flanking pyridyl groups of the **[1$_{CO2Me}$-M]$^{n+}$** derivatives, for which ranges are given from the most negative to most positive $E_{1/2}$ values of these overlapping couples.

Table 1. Analysis of CV data for complexes [1X-Co]$^{n+}$.

X	Avg. $E_{1/2}$ Red1,2[a] (V vs. Fc$^{+/0}$)	$\Delta E_{red1,2}$ (mV)	Avg. $E_{1/2}$ Red3,4[a] (V vs. Fc$^{+/0}$)	$\Delta E_{red3,4}$ (mV)
CO_2Me	-0.90	396	-1.41	308
Cl	-0.89	338	-1.40	284
H	-0.98[b]	272[b]	-1.49[b]	288[b]
Me	-1.00	237	-1.51	280
OMe	-1.01	207	-1.52	260
NMe_2	-1.14	122	-1.65	242

(a) Midpoint value of the first and second reduction potentials (Red1,2) or the third and fourth reduction potentials (Red3,4) listed to the nearest 10 mV. (b) Data from reference 6a.

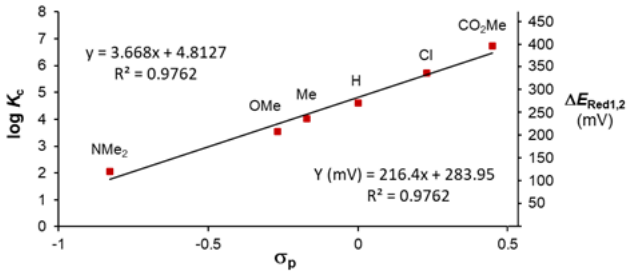

Figure 2. Correlation of the comproportionation constants (log K_c) for the n = 4+ and 2+ states of **[1X-Co]$^{n+}$** with the σ_p Hammet parameter of the-substituents on the flanking pyridyl groups of the ligands. $\Delta E_{Red1,2}$ values are labeled on the right-hand axis.

individual properties of each ligand. Likewise, the midpoint values between E_{red1} and E_{red2} show a good linear correlation with the σ_p values of the pyridyl groups (Figure S57), but an even better correlation was seen between σ_p and the comproportionation constants (log K_c) for the **[1X-Co]$^{4+}$** and **[1X-Co]$^{2+}$** states (Figure 2), which correspond to the strength of coupling between the ligands. This latter observation confirms that control over delocalization is determined by the donor strength of the supporting ligands.

The third and fourth ligand-centered reductions of **[1X-Co]$^{n+}$** also show substantial separation for each derivative, spanning from $\Delta E_{red3,4}$ = 242 mV for **[1NMe2-Co]$^{n+}$** to $\Delta E_{red3,4}$ = 308 mV for **[1CO2Me-Co]$^{n+}$**. Thus, while the $\Delta E_{red3,4}$ values show a trend in the same direction as for the first and second reductions, the overall change is much smaller, and the smallest $\Delta E_{red3,4}$ value observed is nearly twice that of the smallest $\Delta E_{red1,2}$ value (both seen for the NMe_2 derivative). These observations do not have as obvious of an interpretation as for the separations of the more positive redox couples. The large $\Delta E_{red3,4}$ value even for the NMe_2 derivative suggests strong inter-ligand electronic coupling in the mixed-valence **[1NMe2-Co]$^{1+}$** state, which is consistent with the few other known metal-bridged systems that show multiple MV states,[16a,b,29] in which coupling is usually stronger in the more reduced states. However, it is unclear why electronic coupling would be less responsive to tuning in the 1+ state than observed for the 3+ states. This observation could indicate that nearly full delocalization is achieved in the 1+ state of the NMe_2 derivative, leaving little room to increase further, but this seems unlikely since the maximum $\Delta E_{red3,4}$ value in the series is much lower than the maximum $\Delta E_{red1,2}$ value. Instead, the relative invariance of $\Delta E_{red3,4}$ might be due to a complex interplay between the degree of metal-centered reduction and structural changes that viologens undergo in their most reduced states.[30,31]

The NHC ligated cobaltoviologen **[2-Co]$^{5+}$** exhibits CVs that are more similar to those of the **[1X-Zn]$^{4+}$** complexes than to those of the other cobaltoviologens. The first reduction of **[2-Co]$^{5+}$** is a ligand-centered 2 e$^-$ process occurring at $E_{1/2}$ = −0.885 V (Figure 1) with a peak separation of ~120 mV (Figure S68), which is slightly wider than that (~80 mV) observed for the 2 e$^-$ first reduction of the zinc complexes. Likewise, the two subsequent 1 e$^-$ reductions of **[2-Co]$^{n+}$** ($E_{1/2}$ = −1.29, −1.40 V, ΔE = 110 mV) are spaced slightly wider than for the zinc complexes but still much narrower than the separations between the third and fourth ligand-centered reductions of the **[1X-Co]$^{n+}$** series. These data reveal that **[2-Co]$^{n+}$** exhibits much weaker inter-ligand electronic coupling than observed for the terpy-based cobaltoviologens. The differences in electronic delocalization likely arise due to the different oxidation states of cobalt in **[1X-Co]$^{n+}$** and **[2-Co]$^{n+}$**. The NHC-supported cobaltoviologen does not exhibit a Co^{III}/Co^{II} redox couple (Figure S69), so the viologen-like groups are bridged by a Co^{III} center instead of the Co^{II} centers present in the **[1X-Co]$^{n+}$** complexes when their ligands are reduced. The strong electronic coupling in the **[1X-Co]$^{n+}$** series is facilitated by a half-filled 3d orbital that can interact with both viologen π systems.[6a] In contrast, Co^{III} is low spin, leaving the π-symmetry 3d orbitals[32] of **[2-Co]$^{n+}$** fully occupied and unavailable for communicating an electron between the two ligands. The ability to control the oxidation and spin state of cobalt in the cobaltoviologens is a unique feature of these MV systems, representing a novel way to tune inter-ligand electronic coupling.

Returning to the **[1X-Co]$^{n+}$** series, the CO_2Me derivative shows four additional overlapping redox processes negative of −2.0 V vs. Fc$^{+/0}$ that provide additional confirmation of the role of orbital occupancy in promoting delocalization. These redox features, which are also seen for the zinc derivative, can be attributed to reduction of the four electron-deficient flanking pyridyl groups and do not exhibit substantial separation for either the cobalt or zinc complexes. Thus, while the cobalt center in **[1CO2Me-Co]$^{n+}$** is able to electronically couple the viologen moieties, it does not show this effect for the flanking pyridyl groups. Since Co^{II} can have only one of its π-symmetry d orbitals partially occupied, and this orbital couples the viologens,[6a] there is no d orbital available for coupling the flanking pyridyl groups.

Classifying electronic coupling by IVCT band analysis. The comproportionation constants (logK_c = 2.07 to 6.71) observed for the n = 4+ and 2+ states of the **[1X-Co]$^{n+}$** series suggest that there is considerable variation of the strength of electronic coupling between the ligands in the 3+ states

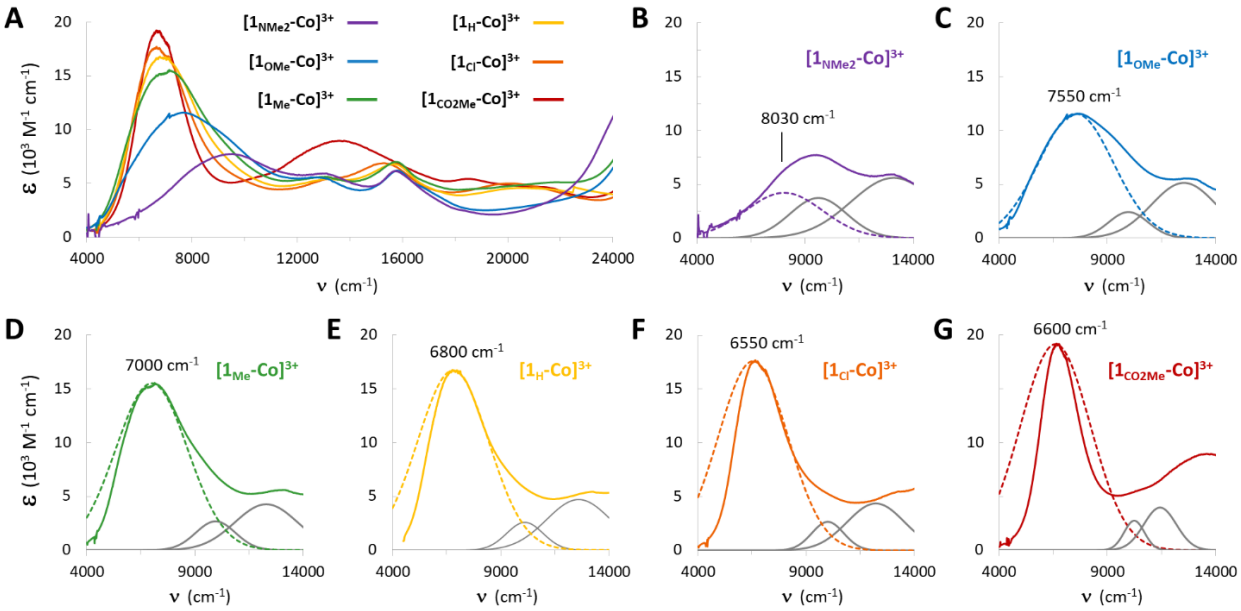

Figure 3. NIR-vis regions of the spectra of **[1X-Co]3+**. (A) Overlay of all spectra in this series. (B – G) IVCT analysis of each spectrum from that of (B) **[1NMe2-Co]3+** to (G) **[1CO2Me-Co]3+**. Solid, colored lines show the experimental spectra, dotted colored lines depict theoretical gaussian IVCT bands with their ε_{max} values indicated, and gray lines depict two freely refined gaussian bands that overlap partially with the IVCT bands (see Figures S94–S99 for full gaussian deconvolution of the NIR-vis regions of these spectra).

of these complexes. However, K_c values can be unreliable for classifying electronic delocalization,[33] so UV-vis-NIR spectroscopy was employed for a clearer analysis. As can be seen in Figure 3A, all the **[1X-Co]3+** complexes exhibit a well-defined intervalence charge-transfer (IVCT) band[3] in the NIR region of their spectra. The intensities of these IVCT bands increase and their widths decrease with increasing EW character of the flanking donor groups of the ligands, consistent with increasing electronic coupling between the ligands.[3]

The IVCT bands were analyzed to assign Robin-Day classifications to each **[1X-Co]3+** complex. We previously classified **[1H-Co]3+** by fitting its IVCT band to a gaussian curve in order to extract the full-width at half max ($\Delta\nu_{1/2}$) of the band and the electronic coupling parameter (H_{ab}),[6a] which both indicate the strength of electronic coupling.[3] Though this approach is commonly used to analyze mixed-valence systems,[10c,11a,16a,b,] it suffers from two major limitations: (1) strongly coupled systems lead to truncation of the IVCT band on its low energy side, so it does not maintain a gaussian shape; and (2) calculating H_{ab} requires the distance (r_{ab}) between the redox sites,[3] which is not well defined in **[1X-Co]3+** since each viologen unit is itself a delocalized π system. Thus, we employed a more sophisticated method of IVCT analysis for comparing electronic coupling in the **[1X-Co]3+** series of complexes.[3a,11d] First, the ε_{max} values of the observed IVCT bands were used to calculate theoretical gaussian IVCT bands assuming Class II coupling.[3a] These theoretically derived bands were combined with four to five freely refined gaussian curves to fit the vis-NIR region of each spectrum (see Figures S94–S99), confirming that features aside from the IVCT bands are relatively consistent for each spectrum. Finally, Robin-Day classifications were assigned by comparing the theoretical and experimental IVCT bands to measure truncation of the latter (Figure 3B–3G), which is directly related to the strength of electronic coupling between the ligands.

As can be seen in Figures 3B,C, the most electron-rich complexes **[1NMe2-Co]3+** and **[1OMe-Co]3+** have IVCT bands that are well matched to theoretical gaussian curves even on the low-energy sides of these absorptions, consistent with Class IIA coupling,[3a] though the high intensity and slight truncation of the IVCT band for **[1OMe-Co]3+** suggests that this complex is at the upper limit of this assignment. The complexes **[1Me-Co]3+**, **[1H-Co]3+**, and **[1Cl-Co]3+** show more noticeable truncation of the low-energy side of their IVCT bands (Figures 3D-F), while excellent consistency is maintained between the experimental and theoretical bands on the high-energy side. The truncation of the IVCT bands increases as the electron-donor strength of the flanking ligands decreases, confirming that electronic delocalization is increased as the orbital energies of the cobalt centers are decreased. Since the IVCT band of **[1Me-Co]3+** is only mildly truncated, we assign this complex to a Class IIB description. It is more difficult to distinguish between Class IIB and borderline Class II/III descriptions for **[1H-Co]3+** and **[1Cl-Co]3+**.[34] Our previous assignment of **[1H-Co]3+** as borderline Class II/III was made using methods employed by others[13c,15a,16a,b] to analyze metal-bridged mixed-valence systems, and adding to this evidence, its IVCT band was found to be invariant to changing the solvent from MeCN to water (Figure S92). This absence of solvatochromism is a strong indicator of a highly delocalized electronic structure,[35] so we maintain our borderline Class II/III description for this complex, and by extension, for **[1Cl-Co]3+**.

Interestingly, the experimental IVCT band of **[1CO2Me-Co]3+** poorly matches the theoretical gaussian band on both the low-energy and high-energy sides of the absorption. Truncation of the IVCT band is not supposed to alter the

band shape on the high energy side,[3] so a different explanation is needed. Since the experimental ν_{max} of the IVCT band is taken as ν_{max} of the theoretical gaussian band, and the width of the gaussian band is derived from ν_{max},[3a] the discrepancy between the experimental and theoretical absorptions suggests that the experimental ν_{max} value is not a good representation of ν_{max} of the corresponding gaussian curve. In other words, these results suggest that the low-energy portion of the experimental IVCT band is truncated to beyond ν_{max} of the theoretical Class II band, just as expected for a Class III mixed-valence system.[3a,b] Comparison of $\Delta\nu_{1/2}$ of the experimental IVCT band with that of the theoretical gaussian band offers another method of evaluating the extent of delocalization. In this case, the experimental full-width at half maximum ($\Delta\nu_{1/2}$ = 2185 cm^{-1}) is 0.57 times that of the theoretical gaussian band ($\Delta\nu_{1/2}$ = 3792 cm^{-1}). This ratio is slightly larger than the ≤ 0.5 limit expected for Class III coupling, but it has been noted that physically realistic IVCT bands are not truncated as sharply as theoretically predicted,[11d] so a value slightly larger than 0.5 is not unreasonable for a Class III system.[10b]

As expected from CV data, full or partial 2 e^- reduction of **[2-Co]$^{5+}$** does not produce spectra showing signs of electronic coupling (Figure 4). Instead, the 3+ spectrum exhibits

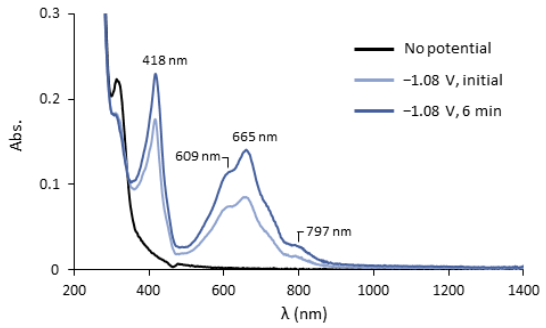

Figure 4. Spectroelectrochemistry of the reduction of **[2-Co]$^{5+}$** to **[2-Co]$^{3+}$** (1 mM in MeCN) at −1.08 V vs. $Fc^{+/0}$ in a 1 mm pathlength cuvette.

features that closely resemble those of fully organic viologen radical cations.[21] In fact, the visible-region absorptions of **[2-Co]$^{3+}$** are even more like those of organic viologen radicals than we reported for the zinc complex **[1$_H$-Zn]$^{2+}$**.[6a] Since **[2-Co]$^{3+}$** is not mixed valence, it is the absence of an IVCT band in the partially reduced sample (Figure 4, −1.08 V, initial) that confirms that the viologen units of **[2-Co]$^{n+}$** are electronically isolated. Notably, this observation extends the electronic coupling in the cobaltoviologens all the way from completely localized Class I to fully delocalized Class III, with considerable gradation between these extremes, thus demonstrating an unprecedented degree of control over delocalization in a constant L-M-L core.

The spectra of the 2+ and 1+ states of the **[1$_X$-Co]$^{n+}$** series were also acquired. As shown in Figures S72, S76, S80, S84, and S89, the 2+ states all have similar vis-NIR features to those reported for **[1$_H$-Co]$^{2+}$**,[6a] with only relatively gradual changes in intensities, λ_{max} values, and band widths, especially from **[1$_{OMe}$-Co]$^{2+}$** to **[1$_{Cl}$-Co]$^{2+}$**, while the NMe_2 and CO_2Me derivatives show somewhat greater differences. The 1+ spectra are also fairly consistent for each complex, with the complexes **[1$_{NMe2}$-Co]$^{+}$** to **[1$_H$-Co]$^{+}$** showing the greatest similarities, while the Cl and CO_2Me derivatives show somewhat broader, more intense bands. Overall, neither the 2+ nor 1+ spectra suggest any dramatic change in the electronic structure across these series, and the changes that are observed for the 1+ complexes are not consistent with changes in inter-ligand electronic coupling. These findings support CV data indicating that electronic coupling does not vary substantially in the 1+ states of these complexes.

Computational insights and limitations. It is challenging to obtain accurate results when computationally modeling delocalization between two redox sites,[3b,36] yet it is not uncommon for DFT to be employed to analyze metal-bridged mixed-valence systems.[10,11a,b,12,14] Thus, we assessed whether common DFT methods could replicate the gradual variation of coupling observed experimentally for the **[1$_X$-Co]$^{3+}$** series. Ultimately, the electronic structures were not described well by these calculations, so we comment only briefly on these results to highlight these limitations and to note one feature of the calculations that did show consistent correlation with experimental results.

Calculations on the **[1$_x$-Co]$^{3+}$** series were first performed using the uB3LYP functional[37] and def2TZVPP basis set for all atoms except C and H, for which def2SVP was used.[38] Antiferromagnetic coupling between Co^{II} and the ligand radical was treated as previously described.[6a] These calculations produce full delocalization of the mixed-valence state for all complexes, failing to match the gradation characterized experimentally. In contrast, employing a IEF-PCM solvent model[39] for MeCN produced wavefunctions that localized the ligand-centered radical to one viologen unit for all complexes. Likewise, the range-separated hybrid functional uCAM-B3LYP, which corrects for the tendency of hybrid functionals to overestimate electronic delocalization,[36,40] produced wavefunctions that were overly localized. Thus, these methods, which have been employed to model other mixed-valence systems,[10a,b,11b,14a,b,15c] were ineffective for **[1$_X$-Co]$^{3+}$**.

Despite poorly modeling delocalization in **[1$_X$-Co]$^{3+}$**, the energy difference between the quintet state of **[1$_X$-Co]$^{3+}$** and its lower energy antiferromagnetically coupled triplet state correlates well with the degree of electronic coupling identified experimentally. In particular, the calculated energy difference $\Delta G_{Q,T}$ scales linearly with the $\log K_c$ of these complexes (Figures S103, S111, S119), establishing a linear free-energy relationship. This correlation may provide a simple method for predicting delocalization in related complexes, and we are pursuing the use of these computational methods in the design of new cobalt-bridged mixed-valence systems. Since substantial effort can be required to accurately model even simple organic viologen radicals,[21a] we regard further computational investigation of the **[1$_X$-Co]$^{3+}$** complexes as outside the scope of this present report.

Single-crystal X-ray diffraction and radical stacking. As we have reported, structural data support the description of **[1$_H$-Co]$^{3+}$** as a nearly fully delocalized mixed-valence system.[6a] Thus, single-crystal XRD characterization of **[1$_H$-**

Co]$^{2+}$ and **[1$_H$-Co]$^{+}$** was carried out to similarly bolster our understanding these states, especially given potential limitations of DFT calculations. The central C—C bond distances and dihedral angles of viologens decrease significantly upon reduction,[21b,31a] so these metrics were compared for **[1$_H$-Co]$^{3+}$** and newly acquired structures of **[1$_H$-Co]$^{2+}$** and **[1$_H$-Co]$^{+}$**. Two crystals of **[1$_H$-Co]**$(PF_6)_2$ were analyzed, one grown from PhCN (R_1 = 4.53 %, Figure 5) and the other from MeCN (R = 8.47 %, Figure 6), with the latter featuring two unique equivalents of **[1$_H$-Co]$^{2+}$**. A single high-quality structure of **[1$_H$-Co]**PF_6 was also determined (R_1 = 4.39 %, see Figure S100). The pyridine-pyridinium (C_{py}–C_{py+}) bonds shorten on going from the 3+ to 2+ and then 1+ states (Table 2), though only the latter change can be distinguished confidently beyond experimental error. The py—py+ dihedral angles decrease significantly between the 3+ and 2+ state, from ~12° in **[1$_H$-Co]$^{3+}$** to ~3° in **[1$_H$-Co]$^{2+}$** (Table 2), consistent with greater reduction of the viologen moieties in the 2+ state. These results confirm the increasing reduction of the ligands for each electron added to **[1$_H$-Co]$^{n+}$**, with the relative subtlety of the changes reflecting the distribution of the effects of each reduction across both ligands.

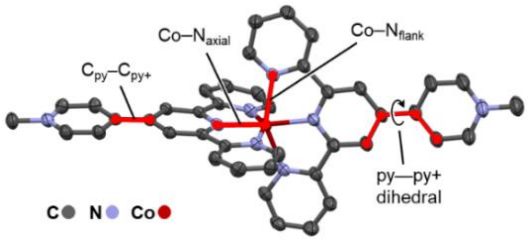

Figure 5. Structure of **[1$_H$-Co]$^{2+}$** determined by XRD (R_1 = 4.53 %) on a single crystal of **[1$_H$-Co]**$(PF_6)_2$ grown by vapor diffusion of Et_2O into a PhCN solution of the salt. Anions and solvates are omitted for clarity. Labels identify the bonds and torsion angles compared in Table 2 for the n = 1 – 3 states of **[1$_H$-Co]$^{n+}$**.

Table 2. Analysis of structural parameters of [1$_X$-Co]$^{n+}$.

Complex	C_{py}–C_{py+} Distance (Å)	py–py+ Dihedral Angle (°)	Co–N$_{axial}$ Distance (Å)	Co–N$_{flank}$ Distance (Å)
[1$_H$-Co]$^{3+}$	1.442(6)[a]	11.1(7)[a]	1.941(3)[a]	2.052(4)[a] 2.062(4)[a]
[1$_H$-Co]$^{2+}$	1.429(5)– 1.439(4)[b]	3.4(6)[c] 3.0(4)[c]	1.978(6)– 2.058(6)[b]	2.131(3)– 1.171(4)[d]
[1$_H$-Co]$^{1+}$	1.412(2) 1.424(2)	0.6(2) 0.8(2)	2.0105(9) 1.9630(9)	2.142(1) 2.150(1) 2.147(1) 2.159(1)

(a) Related to a symmetry-equivalent bond/angle by a 2-fold rotation. (b) Shortest to longest of six distances from three unique **[1$_H$-Co]$^{2+}$** units. (c) Values from the structure of **[1$_H$-Co]**$(PF_6)_2$ without radical pairing interactions. (d) Shortest to longest of twelve distances from three unique **[1$_H$-Co]$^{2+}$** units.

The coordination sphere around cobalt exhibits changes between the 3+ and 2+ states of **[1$_H$-Co]$^{n+}$**, while remaining essentially constant for the 2+ and 1+ states. The Co—N bond distances are all longer in the 2+ structure than in the 3+ structure, suggesting that the cobalt center may be more reduced in **[1$_H$-Co]$^{2+}$** than was indicated in past calculations.[6a] However, neither the 1+ nor 2+ states have particularly long Co—N bonds compared to those of bis-terpy-Co(II) complexes,[25] consistent with the previous assignment of each reduction as centered primarily on the ligands, with moderately increased metal character in the more reduced states of **[1$_H$-Co]$^{n+}$**.

Interestingly, in crystals of **[1$_H$-Co]$^{2+}$** grown from MeCN (**[1$_H$-Co]**$(PF_6)_2$•3.5MeCN), the complexes engage in π-stacking interactions between the viologen ligands that are characteristic of radical pimerization of organic viologens.[21] The asymmetric unit (Figures 6A,B) includes two unique

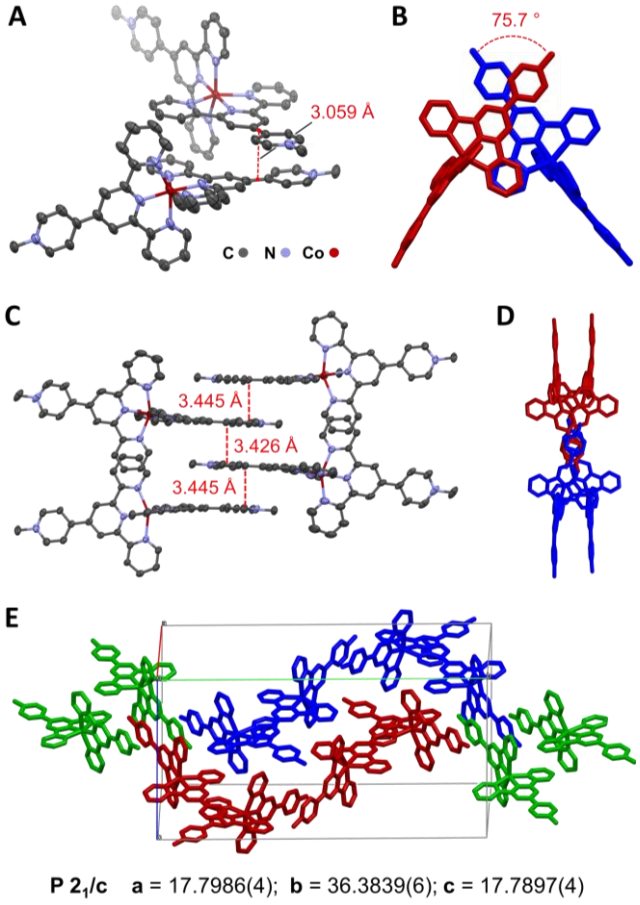

Figure 6. Structure of **[1$_H$-Co]**$(PF_6)_2$•3.5MeCN determined by single-crystal XRD (R_1 = 8.47 %). Anions and solvates are omitted for clarity. (A) Asymmetric unit showing close contact between two crystallographically unique equivalents of **[1$_H$-Co]$^{2+}$**. (B) Top-down view of the stacked viologen ligands in the asymmetric unit. (C) Stacking of four viologen ligands in the extended packing structure. (D) View down the stack of four viologen ligands. Red and blue coloring is used to distinguish alternating equivalents of **[1$_H$-Co]$^{2+}$**. (E) Extended chains of π stacking between **[1$_H$-Co]$^{2+}$** complexes in the unit cell. Red and blue coloring is used to distinguish two separate chains of complexes in the unit cell, and green represents complexes outside the unit cell that unite the two chains in the cell.

[1$_H$-Co]$^{2+}$ complexes, each with a viologen ligand crossing the other at their C_{py}—C_{py+} bonds to give a short centroid-to-centroid contact of 3.06 Å and a dihedral angle of 75.7° between the ligands at this contact. This geometry is nearly ideal for the orbital mixing that produces a weak covalent bonding interaction between organic viologen radicals.[21a,41] Such interactions can facilitate through-space delocalization[42] of electrons across multiple viologens,[22b] yielding unique electronic properties in discrete stacks of viologens[22c-d] and semiconductor behavior in continuous crystalline lattices.[22a] Despite the importance of these interactions in traditional viologen radicals, such behavior has never previously been characterized in metalloviologens, representing a notable fundamental discovery.[43]

The extended packing of the complexes reveals a second notable π-stacking motif (Figures 6C,D) in which four ligands are arranged together with a separation between them (> 3.4 Å) that is characteristic of van der Waals contacts in the absence of radical-pairing. Consistent with this description, overlap of the ligands is limited mostly to the pyridinium groups and occurs at a very wide angle (Figure 6D), yielding poor alignment for mixing the singly occupied orbitals of each ligand. Interestingly, these quadruple stacks of ligands serve as nodes that crosslink separate chains of cobaltoviologen complexes in the extended packing of **[1$_H$-Co]**$(PF_6)_2$•3.5MeCN (Figure 6E). The resulting 3-dimensional network of π stacking appears to impart remarkable elastic flexibility to the bulk crystals,[44] producing needle-like crystals that can recover from being bent by as much as 90° (see supplemental videos). These findings suggest that cobaltoviologens may be useful for developing novel materials. However, crystals of **[1$_H$-Co]**$(PF_6)_2$•3.5MeCN quickly become fragile once removed from their supernatant, so far limiting further scrutiny of their elastic properties.

It is worth noting that one viologen ligand of each **[1$_H$-Co]$^{2+}$** complex engages in strong radical-dimerization while the opposite ligand enters into the quadruple-stack motif with weaker π stacking. The alternating behavior of the ligands might arise from the electronic structure of **[1$_H$-Co]$^{2+}$**, which features one ligand radical coupled ferromagnetically to cobalt while the other couples antiferromagnetically. Since this latter interaction pairs the π* radical with the metal, it may render the ligand unable to participate in intermolecular radical-radical interactions, while leaving available the strong van der Waals forces that also play an important role in viologen pimerization.[21a] Thus, metal-ligand electronic interactions in **[1$_H$-Co]$^{2+}$** may contribute to the packing motif seen in these crystals, and by extension, their unusual physical properties.

The zinc complex **[1$_H$-Zn]$^{2+}$**, which has two radical ligands and a closed-shell metal center, serves as an obvious experimental control for understanding how metal-ligand electronic coupling influences intermolecular radical pairing. Like the cobalt analogue, **[1$_H$-Zn]**$(PF_6)_2$ can be crystallized from MeCN to yield a packing structure defined by radical pimerization (Figure 7), while these interactions are absent in crystals grown from PhCN (Figure S101). However, packing in the MeCN structures differs considerably between the cobalt and zinc derivatives, with the latter engaging both ligands of each complex in radical-pairing interactions, as expected since both ligand radicals should be equivalent in **[1$_H$-Zn]$^{2+}$**. The distance of ~2.99 Å and angle of 80.9° between the stacked ligands are consistent with strong radical pairing, but the extended structure still reveals stacks of four viologens—one viologen unit in each radical dimer also engages in van der Waals contacts (3.399 Å) with one of the viologens of a neighboring radical dimer (Figure 7B). Thus, paired radical ligands maintain the ability to engage in further π stacking, just without the benefit of additional radical-radical interactions.[45] These observations appear to support the conjecture that the reason only one ligand in **[1$_H$-Co]$^{2+}$** engages in strong radical pimerization is that the other ligand π* electron pairs antiferromagnetically with the cobalt center.

The π stacking in **[1$_H$-Zn]**$(PF_6)_2$ provides a 3-dimensionally extended network of stacking interactions, again leading to elastically flexible crystals (see supplemental video). Since the π stacking networks differ considerably between the zinc and cobalt crystals, it seems the combination of radical-pairing and van der Waals interactions may be more important than the specific topology of these interactions for supporting mechanical flexibility. As with the cobalt analogue, the crystals of **[1$_H$-Zn]**$(PF_6)_2$ lose their integrity quickly outside of solvent, preventing further study of their mechanical properties. However, it was possible to use diffuse reflectance UV-vis-NIR spectroscopy to demonstrate that radical pairing interactions are maintained even after degradation of the crystals. An increased NIR absorbance and broadened visible region band, which are both characteristic of viologen radical dimerization,[21a] were observed for dried samples of crystals featuring the radical-pairing motif in comparison to crystals grown under conditions that do not lead to radical pairing (Figure 7C).

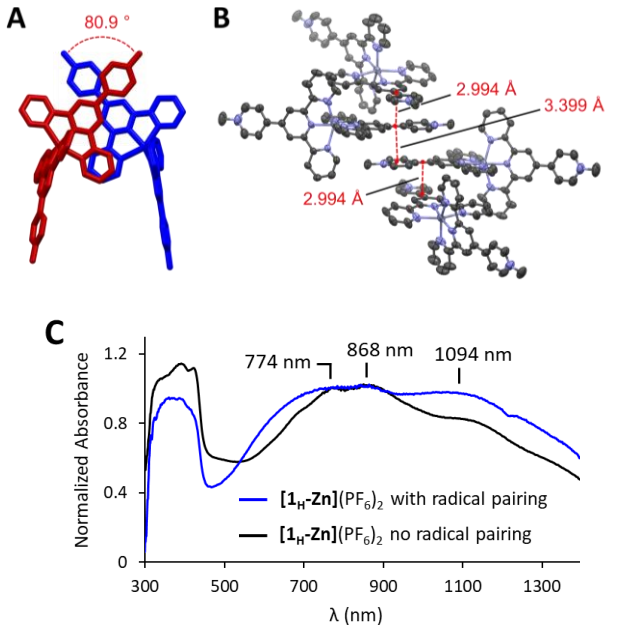

Figure 7. (A) Structure of **[1$_H$-Zn]$^{2+}$** determined by XRD (R_1 = 7.97 %) on a single crystal of **[1$_H$-Zn]**$(PF_6)_2$•3MeCN. The asymmetric unit is shown with anions and solvates omitted. (B) Quadruple-stack of viologen units observed in the extended packing of **[1$_H$-Zn]**$(PF_6)_2$•3MeCN. (C) Diffuse-reflectance UV-vis-NIR spectra of solid-state samples of **[1$_H$-Zn]**$(PF_6)_2$ with and without radical pairing interactions.

Summary and Conclusions.

We have prepared a series of metalloviologen complexes **[1$_X$-M]$^{n+}$** and **[2-Co]$^{5+}$** in which two viologen-like redox units are bridged by either a cobalt or zinc ion. Systematically altering the donor strengths of the supporting ligands in the cobalt complexes afforded remarkable control over electronic coupling between the viologens, representing a novel strategy for altering the delocalization between two organic redox sites. Notably, the mixed-valence states of the cobaltoviologens could be tuned all the way from fully localized Class I to fully delocalized Class III descriptions, providing the first L-M-L system in which this full range of states could be achieved while maintaining a fixed set of redox-active ligands and bridging metal center. The redox properties of the complexes indicate that control over electronic coupling results from modulating the energies of the orbitals on cobalt while leaving the viologen ligands relatively unperturbed. This allows the energies of high-spin Co^{II} orbitals to be matched to those of the ligands to maximize delocalization, while at the other extreme, electronic coupling is turned off when the cobalt center is perturbed enough to change its oxidation state to low-spin Co^{III}.

In addition to the electronic coupling observed between the viologen ligands of a single complex, it was also revealed that these ligands can engage in intermolecular radical-pairing interactions in solid-state structures of **[1$_H$-Co]$^{2+}$** and **[1$_H$-Zn]$^{2+}$**. This finding represents the first time that metalloviologen complexes have been observed to engage radical π-stacking interactions, leading to emergent features that are not observed for such interactions in organic viologens. In particular, both the cobalt and zinc complexes assemble into 3D crystalline networks of π-stacking interactions, leading to mechanically elastic crystals. However, the packing motif differs appreciably between the cobalt and zinc complexes, with the latter engaging both ligands in radical pairing, while the cobalt derivative engages one ligand of each complex in radical-pairing and the other in a weaker type of π stacking. These differences suggest that metal-ligand electronic interactions in the cobalt complex influence the ability of one of the ligand-centered radicals to engage in intermolecular radical dimerization, thus representing another emergent feature arising from metal-ligand electronic interactions in the cobaltoviologens.

ASSOCIATED CONTENT

Supporting Information. Synthetic and experimental procedures; NMR (^{1}H, ^{13}C{^{1}H}), UV-vis-NIR, and ESI(+)-MS spectra; cyclic voltammagrams; single-crystal X-ray diffraction data and analysis; and details of DFT calculations. These materials are available free of charge via the Internet.

AUTHOR INFORMATION

Corresponding Author

* ml1353@chem.rutgers.edu

Author Contributions

All authors have given approval to the final version of the manuscript.

Notes

The authors declare no competing financial interests.

ACKNOWLEDGMENT

The authors acknowledge Rutgers, The State University of New Jersey for financial support of this research; the Office of Advanced Research Computing (OARC) at Rutgers, The State University of New Jersey for providing access to the Amarel cluster and associated research computing resources; and the National Science Foundation under Grant CHE-211772 for supporting the purchase of a single-crystal X-ray diffractometer employed in this research. IFM acknowledges the National Science Foundation Graduate Research Fellowship Program for support via Award DGE-2233066.

REFERENCES

(1) For recent reviews: (a) Heckmann, A.; Lambert, C. Organic Mixed-Valence Compounds: A Playground for Electrons and Holes. *Angew. Chem. Int. Ed.* **2012**, *51*, 326–392. DOI: 10.1002/anie.201100944. (b) Hankache, J.; Wenger, O. S. Organic Mixed Valence. *Chem. Rev.* **2011**, *111*, 5138–5178. DOI: 10.1021/cr100441k. (c) Launay, J.-P. Mixed-Valent Compounds and Their Properties – Recent Developments. *Eur. J. Inorg. Chem.* **2020**, *2020*, 329–341. DOI: 10.1002/ejic.201901180.

(2) (a) Gross, S. T. The Crystal Structure of Pb_3O_4. *J. Am. Chem. Soc.* **1943**, *65*, 1107–1110. DOI: doi.org/10.1021/ja01246a029. (b) Mazej, Z.; Michałowski, T.; Goreshnik, E. A.; Jagličić, Z.; Arčon, I.; Szydłowska, J.; Grochala, W. The first example of a mixed valence ternary compound of silver with random distribution of Ag(i) and Ag(ii) cations. *Dalton Trans.* **2015**, *44,* 10957–10968. DOI: 10.1039/C5DT00740B. (c) Intrator, J. A.; Orchanian, N. M.; Clough, A. J.; Haiges, R.; Marinescu, S. C. Electronically-coupled redox centers in trimetallic cobalt complexes. *Dalton Trans.* **2022**, *51*, 5660 – 5672. DOI: 10.1039/D1DT03404A. (d) Coropceanu, V.; Gruhn, N. E.; Barlow, S.; Lambert, C.; Durivage, J. C.; Bill, T. G.; Nöll, G.; Marder, S. R.; Brédas, J.-L. Electronic Couplings in Organic Mixed-Valence Compounds: The Contribution of Photoelectron Spectroscopy. *J. Am. Chem. Soc.* **2004**, *126*, 2727–2731. DOI: 10.1021/ja039263u. (e) Creutz, C.; Taube, H. Direct Approach to Measuring the Franck-Condon Barrier to Electron Transfer between Metal Ions. *J. Am. Chem. Soc.* **1969**, *91*, 3988–3989. DOI: 10.1021/ja01042a072. (f) Hernández Sánchez, R.; Zheng, S.-L.; Betley, T. A. Ligand Field Strength Mediates Electron Delocalization in Octahedral $[(^HL)_2Fe_6(L')_m]^{n+}$ Clusters. *J. Am. Chem. Soc.* **2015**, *137*, 11126–11143. DOI: 10.1021/jacs.5b06453. (g) Storr, T.; Wasinger, E. C.; Pratt, R. C.; Stack, T. D. P. The Geometric and Electronic Structure of a One-Electron-Oxidized Nickel(II) Bis(Salicylidene)Diamine Complex. *Angew. Chem. Int. Ed.* **2007**, *46*, 5198–5201. DOI: 10.1002/anie.200701194.

(3) (a) Brunschwig, B. S.; Creutz, C.; Sutin, N. Optical Transitions of Symmetrical Mixed-Valence Systems in the Class II–III Transition Regime. *Chem. Soc. Rev.* **2002**, *31* (3), 168–184. DOI: 10.1039/B008034I. (b) D'Alessandro, D. M.; Keene, F. R. Current Trends and Future Challenges in the Experimental, Theoretical and Computational Analysis of Intervalence Charge Transfer (IVCT) Transitions. *Chem. Soc. Rev.* **2006**, *35* (5), 424–440. DOI: 10.1039/B514590M. (c) Demadis, K. D.; Hartshorn, C. M.; Meyer, T. J. The Localized-to-Delocalized Transition in Mixed-Valence Chemistry. *Chem. Rev.* **2001**, *101*, 2655–2686. DOI: 10.1021/cr990413m.

(4) (a) Sampaio, R. N.; Piechota, E. J.; Troian-Gautier, L.; Maurer, A. B.; Hu, K.; Schauer, P. A.; Blair, A. D.; Berlinguette, C. P.; Meyer, G. J. Kinetics Teach That Electronic Coupling Lowers the Free-Energy Change That Accompanies Electron Transfer. *Proc. Natl. Acad. Sci.* **2018**, *115*, 7248–7253. DOI: 10.1073/pnas.1722401115. (b) Luo, Y.; Tran, J. H.; Wächtler, M.;

Schulz, M.; Barthelmes, K.; Winter, A.; Rau, S.; Schubert, U. S.; Dietzek, B. Remote Control of Electronic Coupling – Modification of Excited-State Electron-Transfer Rates in Ru(Tpy)2-Based Donor–Acceptor Systems by Remote Ligand Design. *Chem. Commun.* **2019**, *55*, 2273–2276. DOI: 10.1039/C8CC10075F. (c) Al-Faouri, T.; Buguis, F. L.; Azizi Soldouz, S.; Sarycheva, O. V.; Hussein, B. A.; Mahmood, R.; Koivisto, B. D. Exploring Structure-Property Relationships in a Bio-Inspired Family of Bipodal and Electronically-Coupled Bistriphenylamine Dyes for Dye-Sensitized Solar Cell Applications. *Molecules* **2020**, *25*, 2260. DOI: 10.3390/molecules25092260.

(5) (a) Xie, L. S.; Sun, L.; Wan, R.; Park, S. S.; DeGayner, J. A.; Hendon, C. H.; Dincă, M. Tunable Mixed-Valence Doping toward Record Electrical Conductivity in a Three-Dimensional Metal–Organic Framework. *J. Am. Chem. Soc.* **2018**, *140*, 7411–7414. DOI: 10.1021/jacs.8b03604. (b) Murase, R.; Hudson, T. A.; Aldershof, T. S.; Nguyen, K. V.; Gluschke, J. G.; Kenny, E. P.; Zhou, X.; Wang, T.; van Koeverden, M. P.; Powell, B. J.; Micolich, A. P.; Abrahams, B. F.; D'Alessandro, D. M. Multi-Redox Responsive Behavior in a Mixed-Valence Semiconducting Framework Based on Bis-[1,2,5]-Thiadiazolo-Tetracyanoquinodimethane. *J. Am. Chem. Soc.* **2022**, *144*, 13242–13253. DOI: 10.1021/jacs.2c03794. (c) Ziebel, M. E.; Darago, L. E.; Long, J. R. Control of Electronic Structure and Conductivity in Two-Dimensional Metal–Semiquinoid Frameworks of Titanium, Vanadium, and Chromium. *J. Am. Chem. Soc.* **2018**, *140*, 3040–3051. DOI: 10.1021/jacs.7b13510. (d) Clough, A. J.; Orchanian, N. M.; Skelton, J. M.; Neer, A. J.; Howard, S. A.; Downes, C. A.; Piper, L. F. J.; Walsh, A.; Melot, B. C.; Marinescu, S. C. Room Temperature Metallic Conductivity in a Metal–Organic Framework Induced by Oxidation. *J. Am. Chem. Soc.* **2019**, *141* (41), 16323–16330. DOI: 10.1021/jacs.9b06898. (e) Clough, A. J.; Skelton, J. M.; Downes, C. A.; de la Rosa, A. A.; Yoo, J. W.; Walsh, A.; Melot, B. C.; Marinescu, S. C. Metallic Conductivity in a Two-Dimensional Cobalt Dithiolene Metal–Organic Framework. *J. Am. Chem. Soc.* **2017**, *139* (31), 10863–10867. DOI: 10.1021/jacs.7b05742.

(6) (a) Mansoor, I. F.; Wozniak, D. I.; Wu, Y.; Lipke, M. C. A Delocalized Cobaltoviologen with Seven Reversibly Accessible Redox States and Highly Tunable Electrochromic Behaviour. *Chem. Commun.* **2020**, *56*, 13864–13867. DOI: 10.1039/D0CC05627H. (b) Cui, B.-B.; Tang, J.-H.; Yao, J.; Zhong, Y.-W. A Molecular Platform for Multistate Near-Infrared Electrochromism and Flip-Flop, Flip-Flap-Flop, and Ternary Memory. *Angew. Chem. Int. Ed.* **2015**, *54*, 9192–9197. DOI: 10.1002/anie.201504584. (c) Rogez, G.; Marvilliers, A.; Sarr, P.; Parsons, S.; Teat, S. J.; Ricard, L.; Mallah, T. Tuning the Optical Properties of Prussian Blue-like Complexes. *Chem. Commun.* **2002**, No. 14, 1460–1461. DOI: 10.1039/B202288E. (d) Weyland, T.; Ledoux, I.; Brasselet, S.; Zyss, J.; Lapinte, C. Nonlinear Optical Properties of Redox-Active Mono-, Bi-, and Trimetallic σ-Acetylide Complexes Connected through a Phenyl Ring in the Cp*(Dppe)Fe Series. An Example of Electro-Switchable NLO Response. Organometallics 2000, 19, 5235–5237. DOI: 10.1021/om0005708.

(7) (a) Kaim, W.; Klein, A.; Glöckle, M. Exploration of Mixed-Valence Chemistry: Inventing New Analogues of the Creutz-Taube Ion. *Acc. Chem. Res.* **2000**, *33* (11), 755–763. DOI: 10.1021/ar960067k. (b) Silva, W. C.; Lima, J. B.; Moreira, I. S.; Neto, A. M.; Gandra, F. C. G.; Ferreira, A. G.; McGarvey, B. R.; Franco, D. W. 4,4'-Dithiodipyridine as a Bridging Ligand in Osmium and Ruthenium Complexes: The Electron Conductor Ability of the −S−S− Bridge. *Inorg. Chem.* **2003**, *42* (21), 6898–6906. DOI: 10.1021/ic034630o.

(8) (a) Gao, H.; Mallick, S.; Cao, L.; Meng, M.; Cheng, T.; Chen, H. W.; Liu, C. Y. Electronic Coupling and Electron Transfer between Two Mo_2 Units through Meta- and Para-Phenylene Bridges. *Chem. – Eur. J.* **2019**, *25*, 3930–3938. DOI: 10.1002/chem.201805866. (b) Patoux, C.; Launay, J.-P.; Beley, M.; Chodorowski-Kimmes, S.; Collin, J.-P.; James, S.; Sauvage, J.-P. Long-Range Electronic Coupling in Bis(Cyclometalated) Ruthenium Complexes. *J. Am. Chem. Soc.* **1998**, *120*, 3717–3725. DOI: 10.1021/ja974137+. (c) Sutton, J. E.; Taube, H. Metal to Metal Interactions in Weakly Coupled Mixed-Valence Complexes Based on Ruthenium Ammines. *Inorg. Chem.* **1981**, *20* (10), 3125–3134. DOI: 10.1021/ic50224a001.

(9) (a) Shao, J.-Y.; Zhong, Y.-W. Tuning the Electronic Coupling in Cyclometalated Diruthenium Complexes through Substituent Effects: A Correlation between the Experimental and Calculated Results. *Chem. – Eur. J.* **2014**, *20* (28), 8702–8713. DOI: 10.1002/chem.201402252. (b) Kundu, T.; Schweinfurth, D.; Sarkar, B.; Mondal, T. K.; Fiedler, J.; Mobin, S. M.; Puranik, V. G.; Kaim, W.; Lahiri, G. K. Strong Metal–Metal Coupling in Mixed-Valent Intermediates $[Cl(L)Ru(\mu\text{-}Tppz)Ru(L)Cl]^{+}$, L = β-Diketonato Ligands, Tppz = 2,3,5,6-Tetrakis(2-Pyridyl)Pyrazine. *Dalton Trans.* **2012**, *41* (43), 13429–13440. DOI: 10.1039/C2DT31763J. (c) Scheiring, T.; Kaim, W.; Olabe, J. A.; Parise, A. R.; Fiedler, J. The Valence-Localized Decacyanodiruthenium(III,II) Analogue of the Creutz–Taube Ion. Completing the Full D^5/D^6 Triad $[(NC)_5M(\mu\text{-}Pz)M(CN)_5]^{5-}$, M=Fe,Ru,Os; Pz=pyrazine. *Inorganica Chimica Acta* **2000**, *300–302*, 125–130. DOI: 10.1016/S0020-1693(99)00456-9. (d) Vance, F. W.; Slone, R. V.; Stern, C. L.; Hupp, J. T. Comparative Absorption, Electroabsorption and Electrochemical Studies of Intervalence Electron Transfer and Electronic Coupling in Cyanide-Bridged Bimetallic Systems: Ancillary Ligand Effects. Chem. Phys. 2000, 253, 313–322. DOI: 10.1016/S0301-0104(99)00400-0.

(10) (a) Hansmann, M. M.; Melaimi, M.; Bertrand, G. Organic Mixed Valence Compounds Derived from Cyclic (Alkyl)(Amino)Carbenes. *J. Am. Chem. Soc.* **2018**, *140*, 2206–2213. DOI: 10.1021/jacs.7b11184. (b) Barlow, S.; Risko, C.; Odom, S. A.; Zheng, S.; Coropceanu, V.; Beverina, L.; Brédas, J.-L.; Marder, S. R. Tuning Delocalization in the Radical Cations of 1,4-Bis[4-(Diarylamino)Styryl]Benzenes, 2,5-Bis[4-(Diarylamino)Styryl]Thiophenes, and 2,5-Bis[4-(Diarylamino)Styryl]Pyrroles through Substituent Effects. *J. Am. Chem. Soc.* **2012**, *134*, 10146–10155. DOI: 10.1021/ja3023048. (c) Yu, C.-H.; Zhu, C.; Ji, X.; Hu, W.; Xie, H.; Bhuvanesh, N.; Fang, L.; Ozerov, O. V. Palladium Bis-Pincer Complexes with Controlled Rigidity and Inter-Metal Distance. *Inorg. Chem. Front.* **2020**, *7*, 4357–4366. DOI: 10.1039/D0QI01111H.

(11) (a) Schäfer, J.; Holzapfel, M.; Mladenova, B.; Kattnig, D.; Krummenacher, I.; Braunschweig, H.; Grampp, G.; Lambert, C. Hole Transfer Processes in Meta- and Para-Conjugated Mixed Valence Compounds: Unforeseen Effects of Bridge Substituents and Solvent Dynamics. *J. Am. Chem. Soc.* **2017**, *139*, 6200–6209. DOI: 10.1021/jacs.7b01650. (b) Jung, H. W.; Yoon, S. E.; Carroll, P. J.; Gau, M. R.; Therien, M. J.; Kang, Y. K. Distance Dependence of Electronic Coupling in Rigid, Cofacially Compressed, π-Stacked Organic Mixed-Valence Systems. *J. Phys. Chem. B* **2020**, *124*, 1033–1048. DOI: 10.1021/acs.jpcb.9b09578. (c) Rovira, C.; Ruiz-Molina, D.; Elsner, O.; Vidal-Gancedo, J.; Bonvoisin, J.; Launay, J.-P.; Veciana, J. Influence of Topology on the Long-Range Electron-Transfer Phenomenon. *Chem. – Eur. J.* **2001**, *7*, 240–250. DOI: 10.1002/1521-3765(20010105)7:1<240::AID-CHEM240>3.0.CO;2-H. (d) Lambert, C.; Nöll, G. The Class II/III Transition in Triarylamine Redox Systems. *J. Am. Chem. Soc.* **1999**, *121* (37), 8434–8442. DOI: 10.1021/ja991264s.

(12) Lambert, C.; Amthor, S.; Schelter, J. From Valence Trapped to Valence Delocalized by Bridge State Modification in Bis(Triarylamine) Radical Cations: Evaluation of Coupling Matrix Elements in a Three-Level System. *J. Phys. Chem. A* **2004**, *108*, 6474–6486. DOI: 10.1021/jp048449s.

(13) (a) Jones, S. C.; Coropceanu, V.; Barlow, S.; Kinnibrugh, T.; Timofeeva, T.; Brédas, J.-L.; Marder, S. R. Delocalization in Platinum–Alkynyl Systems: A Metal-Bridged Organic Mixed-Valence Compound. *J. Am. Chem. Soc.* **2004**, *126*, 11782–11783. DOI: 10.1021/ja045869m. (b) Kojima, T.; Ogishima, F.; Nishibu, T.; Kotani, H.; Ishizuka, T.; Okajima, T.; Nozawa, S.; Shiota, Y.; Yoshizawa, K.; Ohtsu, H.; Kawano, M.; Shiga, T.; Oshio, H. Intermediate-Spin Iron(III) Complexes Having a Redox-Noninnocent Macrocyclic Tetraamido Ligand. *Inorg. Chem.* **2018**, *57*, 9683–9695. DOI: 10.1021/acs.inorgchem.8b00037. (c) Lu, C. C.; Bill, E.; Weyhermüller, T.; Bothe, E.; Wieghardt, K. Neutral Bis(α-Iminopyridine)Metal

Complexes of the First-Row Transition Ions (Cr, Mn, Fe, Co, Ni, Zn) and Their Monocationic Analogues: Mixed Valency Involving a Redox Noninnocent Ligand System. *J. Am. Chem. Soc.* **2008**, *130*, 3181–3197. DOI: 10.1021/ja710663n.

(14) (a) Chiang, L.; Kochem, A.; Jarjayes, O.; Dunn, T. J.; Vezin, H.; Sakaguchi, M.; Ogura, T.; Orio, M.; Shimazaki, Y.; Thomas, F.; Storr, T. Radical Localization in a Series of Symmetric Ni^{II} Complexes with Oxidized Salen Ligands. *Chem. – Eur. J.* **2012**, *18*, 14117–14127. DOI: 10.1002/chem.201201410. (b) Chiang, L.; Herasymchuk, K.; Thomas, F.; Storr, T. Influence of Electron-Withdrawing Substituents on the Electronic Structure of Oxidized Ni and Cu Salen Complexes. *Inorg. Chem.* **2015**, *54*, 5970–5980. DOI: 10.1021/acs.inorgchem.5b00783. (c) Shimazaki, Y.; Stack, T. D. P.; Storr, T. Detailed Evaluation of the Geometric and Electronic Structures of One-Electron Oxidized Group 10 (Ni, Pd, and Pt) Metal(II)-(Disalicylidene)Diamine Complexes. *Inorg. Chem.* **2009**, *48* (17), 8383–8392. DOI: 10.1021/ic901003q.

(15) (a) Yu, C.-H.; Yang, X.; Ji, X.; Wang, C.-H.; Lai, Q.; Bhuvanesh, N.; Ozerov, O. V. Redox Communication between Two Diarylamido/Bis(Phosphine) (PNP)M Moieties Bridged by Ynediyl Linkers (M = Ni, Pd, Pt). *Inorg. Chem.* **2020**, *59*, 10153–10162. DOI: 10.1021/acs.inorgchem.0c01281. (b) Hewage, J. S.; Wanniarachchi, S.; Morin, T. J.; Liddle, B. J.; Banaszynski, M.; Lindeman, S. V.; Bennett, B.; Gardinier, J. R. Homoleptic Nickel(II) Complexes of Redox-Tunable Pincer-Type Ligands. *Inorg. Chem.* **2014**, *53*, 10070–10084. DOI: 10.1021/ic500657e. (c) Liddle, B. J.; Wanniarachchi, S.; Hewage, J. S.; Lindeman, S. V.; Bennett, B.; Gardinier, J. R. Electronic Communication Across Diamagnetic Metal Bridges: A Homoleptic Gallium(III) Complex of a Redox-Active Diarylamido-Based Ligand and Its Oxidized Derivatives. *Inorg. Chem.* **2012**, *51*, 12720–12728. DOI: 10.1021/ic301437f.

(16) (a) Arnold, A.; Sherbow, T. J.; Bohanon, A. M.; Sayler, R. I.; Britt, R. D.; Smith, A. M.; Fettinger, J. C.; Berben, L. A. Delocalization Tunable by Ligand Substitution in $[L_2Al]^{N-}$ Complexes Highlights a Mechanism for Strong Electronic Coupling. *Chem Sci* **2021**, *12*, 675–682. DOI: D0SC02812F. (b) Arnold, A.; Sherbow, T. J.; Sayler, R. I.; Britt, R. D.; Thompson, E. J.; Muñoz, M. T.; Fettinger, J. C.; Berben, L. A. Organic Electron Delocalization Modulated by Ligand Charge States in $[L_2M]^{n-}$ Complexes of Group 13 Ions. *J. Am. Chem. Soc.* **2019**, *141*, 15792–15803. DOI: 10.1021/jacs.9b05602. (c) de Bruin, B.; Bill, E.; Bothe, E.; Weyhermüller, T.; Wieghardt, K. Molecular and Electronic Structures of Bis(Pyridine-2,6-Diimine)Metal Complexes $[ML_2](PF_6)_n$ (n = 0, 1, 2, 3; M = Mn, Fe, Co, Ni, Cu, Zn). *Inorg. Chem.* **2000**, *39*, 2936–2947. DOI: 10.1021/ic000113j.

(17) (a) Ray, K.; Begum, A.; Weyhermüller, T.; Piligkos, S.; van Slageren, J.; Neese, F.; Wieghardt, K. The Electronic Structure of the Isoelectronic, Square-Planar Complexes $[Fe^{II}(L)_2]^{2-}$ and $[Co^{III}(L^{Bu})_2]^-$ (L^{2-} and $(L^{Bu})^{2-}$ = Benzene-1,2-Dithiolates): An Experimental and Density Functional Theoretical Study. *J. Am. Chem. Soc.* **2005**, *127*, 4403–4415. DOI: 10.1021/ja042803i. (b) Vogler, A.; Kunkely, H. A 1,2-Dithiolenenickel Complex with Different Substituents-a Novel Type of Mixed-Valence Compounds. *Angew. Chem. Int. Ed. Engl.* **1982**, *21*, 77. DOI: 10.1002/anie.198200771. (c) Wan, H. C.; Zhang, J.-X.; Leung, C. S.; Sheong, F. K.; Lin, Z. Inter-Ligand Delocalisations in Transition Metal Complexes Containing Multiple Non-Innocent Ligands. *Dalton Trans.* **2019**, *48* (39), 14801–14807. DOI: 10.1039/C9DT02806D.

(18) It is worth clarifying that cobalt bis-dithiolene complexes are not usually described in terms of mixed valency, but the resonance structures $[Co^{III}(L)_2]^- \leftrightarrow [Co^{II}(L)(L^{\bullet})]^- \leftrightarrow [Co^{II}(L^{\bullet})(L)]^-$ presented in reference 17a can be understood as corresponding to a delocalized MV system with considerable bridge-centered redox character.

(19) (a) Römelt, C.; Weyhermüller, T.; Wieghardt, K. Structural Characteristics of Redox-Active Pyridine-1,6-Diimine Complexes: Electronic Structures and Ligand Oxidation Levels. *Coord. Chem. Rev.* **2019**, *380*, 287–317. DOI: 10.1016/j.ccr.2018.09.018. (b) Clarke, R. M.; Herasymchuk, K.; Storr, T. Electronic Structure Elucidation in Oxidized Metal–Salen Complexes. *Coord. Chem. Rev.* **2017**, *352*, 67–82. DOI: 10.1016/j.ccr.2017.08.019. (c) Eisenberg, R.; Gray, H. B. Noninnocence in Metal Complexes: A Dithiolene Dawn. *Inorg. Chem.* **2011**, *50*, 9741 - 9751. DOI: 10.1021/ic2011748.

(20) (a) Chen, K.; Downes, C. A.; Schneider, E.; Goodpaster, J. D.; Marinescu, S. C. Improving and Understanding the Hydrogen Evolving Activity of a Cobalt Dithiolene Metal–Organic Framework. *ACS Appl. Mater. Interfaces* **2021**, *13*, 16384–16395. DOI: 10.1021/acsami.1c01727. (b) Downes, C. A.; Marinescu, S. C. Efficient Electrochemical and Photoelectrochemical H_2 Production from Water by a Cobalt Dithiolene One-Dimensional Metal–Organic Surface. *J. Am. Chem. Soc.* **2015**, *137*, 13740–13743. DOI: 10.1021/jacs.5b07020.

(21) (a) Geraskina, M. R.; Dutton, A. S.; Juetten, M. J.; Wood, S. A.; Winter, A. H. The Viologen Cation Radical Pimer: A Case of Dispersion-Driven Bonding. *Angew. Chem. Int. Ed.* **2017**, *56*, 9435–9439. DOI: 10.1002/anie.201704959. (b) Bockman, T. M.; Kochi, J. K. Isolation and Oxidation-Reduction of Methylviologen Cation Radicals. Novel Disproportionation in Charge-Transfer Salts by x-ray Crystallography. *J. Org. Chem.* **1990**, *55*, 4127–4135. DOI: 10.1021/jo00300a033. (c) Geuder, W.; Hünig, S.; Suchy, A. Single and Double Bridged Viologenes and Intramolecular Pimerization of Their Cation Radicals. *Tetrahedron* **1986**, *42*, 1665–1677. DOI: 10.1016/S0040-4020(01)87583-9.

(22) (a) Fahrenbach, A. C.; Sampath, S.; Late, D. J.; Barnes, J. C.; Kleinman, S. L.; Valley, N.; Hartlieb, K. J.; Liu, Z.; Dravid, V. P.; Schatz, G. C.; Van Duyne, R. P.; Stoddart, J. F. A Semiconducting Organic Radical Cationic Host–Guest Complex. *ACS Nano* **2012**, *6*, 9964–9971. DOI: 10.1021/nn303553z. (b) Barnes, J. C.; Fahrenbach, A. C.; Cao, D.; Dyar, S. M.; Frasconi, M.; Giesener, M. A.; Benítez, D.; Tkatchouk, E.; Chernyashevskyy, O.; Shin, W. H.; Li, H.; Sampath, S.; Stern, C. L.; Sarjeant, A. A.; Hartlieb, K. J.; Liu, Z.; Carmieli, R.; Botros, Y. Y.; Choi, J. W.; Slawin, A. M. Z.; Ketterson, J. B.; Wasielewski, M. R.; Goddard, W. A.; Stoddart, J. F. A Radically Configurable Six-State Compound. *Science* **2013**, *339*, 429–433. DOI: 10.1126/science.1228429. (c) Buck, A. T.; Paletta, J. T.; Khindurangala, S. A.; Beck, C. L.; Winter, A. H. A Noncovalently Reversible Paramagnetic Switch in Water. *J. Am. Chem. Soc.* **2013**, *135*, 10594–10597. https://doi.org/10.1021/ja403505z. (d) Lipke, M. C.; Wu, Y.; Roy, I.; Wang, Y.; Wasielewski, M. R.; Stoddart, J. F. Shuttling Rates, Electronic States, and Hysteresis in a Ring-in-Ring Rotaxane. *ACS Cent. Sci.* **2018**, *4*, 362–371. DOI: 10.1021/acscentsci.7b00535. (e) Feng, L.; Qiu, Y.; Guo, Q.-H.; Chen, Z.; Seale, J. S. W.; He, K.; Wu, H.; Feng, Y.; Farha, O. K.; Astumian, R. D.; Stoddart, J. F. Active Mechanisorption Driven by Pumping Cassettes. *Science* **2021**, *374*, 1215–1221. DOI: 10.1126/science.abk1391. (f) Palmquist, M. S.; Gruschka, M. C.; Dorsainvil, J. M.; Delawder, A. O.; Saak, T. M.; Danielson, M. K.; Barnes, J. C. Electrostatic Loading and Photoredox-Based Release of Molecular Cargo from Oligoviologen-Crosslinked Microparticles. *Polym. Chem.* **2022**, *13*, 2115–2122. DOI: 10.1039/D2PY00249C. (g) Greene, A. F.; Danielson, M. K.; Delawder, A. O.; Liles, K. P.; Li, X.; Natraj, A.; Wellen, A.; Barnes, J. C. Redox-Responsive Artificial Molecular Muscles: Reversible Radical-Based Self-Assembly for Actuating Hydrogels. *Chem. Mater.* **2017**, *29*, 9498–9508. DOI: 10.1021/acs.chemmater.7b03635.

(23) Constable, E. C.; Housecroft, C. E.; Kulke, T.; Lazzarini, C.; Schofield, E. R.; Zimmermann, Y. Redistribution of Terpy Ligands—Approaches to New Dynamic Combinatorial Libraries. *J. Chem. Soc. Dalton Trans.* **2001**, 2864–2871. DOI: 10.1039/B104865C.

(24) Constable, E. C.; Housecroft, C. E.; Neuburger, M.; Phillips, D.; Raithby, P. R.; Schofield, E.; Sparr, E.; Tocher, D. A.; Zehnder, M.; Zimmermann, Y. Development of Supramolecular Structure through Alkylation of Pendant Pyridyl Functionality. *J Chem Soc Dalton Trans* **2000**, 2219–2228. DOI: 10.1039/B000940G.

(25) Aroua, S.; Todorova, T. K.; Hommes, P.; Chamoreau, L.-M.; Reissig, H.-U.; Mougel, V.; Fontecave, M. Synthesis, Characterization, and DFT Analysis of Bis-Terpyridyl-Based Molecular Cobalt Complexes. *Inorg. Chem.* **2017**, *56*, 5930–5940. DOI: 10.1021/acs.inorgchem.7b00595.

(26) Wang, J.; Hanan, G. S. A Facile Route to Sterically Hindered and Non-Hindered 4′-Aryl-2,2′:6′,2′′-Terpyridines. *Synlett* **2005**, *2005*, 1251–1254. DOI: 10.1055/s-2005-868481.

(27) Kobayashi, M.; Masaoka, S.; Sakai, K. Synthesis, Crystal Structure, Spectroscopic and Electrochemical Properties, and H_2-Evolving Activity of a New $[PtCl(Terpyridine)]^+$ Derivative with Viologen-like Redox Properties. *Dalton Trans* **2012**, *41*, 4903–4911. 10.1039/C2DT12209J.

(28) (a) Evans, C. E. B.; Naklicki, M. L.; Rezvani, A. R.; White, C. A.; Kondratiev, V. V.; Crutchley, R. J. An Investigation of Superexchange in Dinuclear Mixed-Valence Ruthenium Complexes. *J. Am. Chem. Soc.* **1998**, *120*, 13096–13103. DOI: 10.1021/ja982673b. (b) Crutchley, R. J. Intervalence Charge Transfer and Electron Exchange Studies of Dinuclear Ruthenium Complexes. In *Advances in Inorganic Chemistry*; Sykes, A. G., Ed.; Academic Press, 1994; Vol. 41, pp 273–325. DOI: 10.1016/S0898-8838(08)60174-9.

(29) (a) Tanaka, M.; Kariya, N.; Abe, M.; Sasaki, Y. Remarkable Stabilization of a Ligand-Based Mixed-Valence State in the Metal-Based Mixed Valent $Ru_2^{II,III}M^{II}$ (μ_3-O) (M = Co, Ni) Trinuclear Cluster Complexes. *BCSJ* **2007**, *80*, 192–194. DOI: 10.1246/bcsj.80.192. (b) Abe, M.; Sasaki, Y.; Yamada, Y.; Tsukahara, K.; Yano, S.; Yamaguchi, T.; Tominaga, M.; Taniguchi, I.; Ito, T. Oxo-Centered Mixed-Ligand Triruthenium Complexes Having Redox-Active N-Methyl-4,4′-Bipyridinium Ions (Mbpy+). Reversible Multistep Electrochemical Properties of $[Ru^{III}_2Ru^{II}(M_3\text{-}O)(\mu\text{-}CH_3CO_2)_6(Mbpy^+)_2(CO)]^{2+}$ and $[Ru^{III}_3(M_3\text{-}O)(\mu\text{-}CH_3CO_2)_6(Mbpy^+)_2(L)]^{3+}$ (L = H_2O and N-Heterocyclic Ligands). *Inorg. Chem.* **1996**, *35*, 6724–6734. https://doi.org/10.1021/ic960430j.

(30) Viologens exhibit pyramidalization of the nitrogen atoms in their most reduced state (ref. 31a,b), which might lead to greater ligand-centered vs. metal-centered reduction in the most reduced states of $\mathbf{[1_x\text{-}Co]^{n+}}$, lowering the influence of ancillary ligands on the n = 1+/0 redox couple.

(31) (a) Frasconi, M.; Fernando, I. R.; Wu, Y.; Liu, Z.; Liu, W.-G.; Dyar, S. M.; Barin, G.; Wasielewski, M. R.; Goddard, W. A. I.; Stoddart, J. F. Redox Control of the Binding Modes of an Organic Receptor. *J. Am. Chem. Soc.* **2015**, *137*, 11057–11068. DOI: 10.1021/jacs.5b05618. (b) Porter, W. W.; Vaid, T. P.; Rheingold, A. L. Synthesis and Characterization of a Highly Reducing Neutral "Extended Viologen" and the Isostructural Hydrocarbon 4,4′ "′-Di-n-Octyl-*p*-Quaterphenyl. *J. Am. Chem. Soc.* **2005**, *127*, 16559–16566. DOI: 10.1021/ja053084q.

(32) The 3d orbitals that can couple the viologen π systems are of e symmetry in the S_4 point group of $\mathbf{[1_X\text{-}Co]^{n+}}$ and $\mathbf{[2\text{-}Co]^{n+}}$.

(33) D'Alessandro, D. M.; Keene, F. R. A Cautionary Warning on the Use of Electrochemical Measurements to Calculate Comproportionation Constants for Mixed-Valence Compounds. *Dalton Trans.* **2004**, 3950–3954. DOI: 10.1039/B413980A.

(34) Conflicting data is often seen for borderline Class II/III coupling. The $\Delta\nu_{1/2}$ values of the IVCT bands of $\mathbf{[1_H\text{-}Co]^{3+}}$ and $\mathbf{[1_{Cl}\text{-}Co]^{3+}}$ suggest Class IIB descriptions (ref. 3a), but assignment as borderline Class II/III or Class III descriptions is supported by the experimental structure (ref. 6a) and lack of solvatochromism in $\mathbf{[1_H\text{-}Co]^{3+}}$, and by comparisons with data for other complexes assigned as Class II/III descriptions (ref. 13a, 15a, 16a,b).

(35) (a) D'Alessandro, D. M.; Keene, F. R. Intervalence Charge Transfer (IVCT) in Trinuclear and Tetranuclear Complexes of Iron, Ruthenium, and Osmium. *Chem. Rev.* **2006**, *106*, 2270–2298. DOI: 10.1021/cr050010o. (b) Chen, P.; Meyer, T. J. Medium Effects on Charge Transfer in Metal Complexes. *Chem. Rev.* **1998**, *98*, 1439–1478. DOI: 10.1021/cr941180w.

(36) (a) Renz, M.; Theilacker, K.; Lambert, C.; Kaupp, M. A Reliable Quantum-Chemical Protocol for the Characterization of Organic Mixed-Valence Compounds. *J. Am. Chem. Soc.* **2009**, *131*, 16292–16302. DOI: 10.1021/ja9070859. (b) Kaupp, M.; Renz, M.; Parthey, M.; Stolte, M.; Wurthner, F.; Lambert, C. Computational and spectroscopic studies of organic mixed-valence compounds: where is the charge? *Phys. Chem. Chem. Phys.* **2011**, *13*, 16973 - 16986. (c) Parthey, M.; Kaupp, M. Quantum-chemical insights into mixed-valence systems: within and beyond the Robin–Day scheme. *Chem. Soc. Rev.* **2014**, *43*, 5067 – 5067. DOI: 10.1039/C3CS60481K.

(37) Stephens, P. J.; Devlin, F. J.; Chabalowski, C. F.; Frisch, M. J. Ab Initio Calculation of Vibrational Absorption and Circular Dichroism Spectra Using Density Functional Force Fields. *J. Phys. Chem.* **1994**, *98*, 11623–11627. DOI: 10.1021/j100096a001.

(38) Weigend, F.; Ahlrichs, R. Balanced Basis Sets of Split Valence, Triple Zeta Valence and Quadruple Zeta Valence Quality for H to Rn: Design and Assessment of Accuracy. *Phys Chem Chem Phys* **2005**, *7*, 3297–3305. DOI: 10.1039/B508541A.

(39) Mennucci, B.; Cancès, E.; Tomasi, J. Evaluation of Solvent Effects in Isotropic and Anisotropic Dielectrics and in Ionic Solutions with a Unified Integral Equation Method: Theoretical Bases, Computational Implementation, and Numerical Applications. *J. Phys. Chem. B* **1997**, *101*, 10506–10517. DOI: 10.1021/jp971959k.

(40) Yanai, T.; Tew, D. P.; Handy, N. C. A New Hybrid Exchange–Correlation Functional Using the Coulomb-Attenuating Method (CAM-B3LYP). *Chem. Phys. Lett.* **2004**, *393*, 51–57. DOI: 10.1016/j.cplett.2004.06.011.

(41) Juneau, A.; Frenette, M. Exploring Curious Covalent Bonding: Raman Identification and Thermodynamics of Perpendicular and Parallel Pancake Bonding (Pimers) of Ethyl Viologen Radical Cation Dimers. *J. Phys. Chem. B* **2021**, *125*, 10805–10812. DOI: 10.1021/acs.jpcb.1c06283.

(42) Orbital descriptions for through-space coupling are the same for mixed-valence and homovalent pimerization: (a) Garcia-Yoldi, I.; Miller, J. S.; Novoa, J. J. Theoretical Study of the Electronic Structure of [Tetrathiafulvalene]22+ Dimers and Their Long, Intradimer Multicenter Bonding in Solution and the Solid State. *J. Phys. Chem. A* **2009**, *113*, 484–492. DOI: 10.1021/jp807022h. (b) Rosokha, S. V.; Kochi, J. K. Molecular and Electronic Structures of the Long-Bonded π-Dimers of Tetrathiafulvalene Cation-Radical in Intermolecular Electron Transfer and in (Solid-State) Conductivity. *J. Am. Chem. Soc.* **2007**, *129*, 828–838. DOI: 10.1021/ja064166x. (c) Kochi, J. K.; Rathore, R.; Maguères, P. L. Stable Dimeric Aromatic Cation–Radicals. Structural and Spectral Characterization of Through-Space Charge Delocalization. *J. Org. Chem.* **2000**, *65*, 6826–6836. DOI: 10.1021/jo000570h.

(43) Mixed-valence pimerization has been enforced in supramolecular metallamacrocycles featuring related 4,4'-bipyryidine ligands: (a) Dinolfo, P. H.; Williams, M. E.; Stern, C. L.; Hupp, J. T. Rhenium-Based Molecular Rectangles as Frameworks for Ligand-Centered Mixed Valency and Optical Electron Transfer. *J. Am. Chem. Soc.* **2004**, *126*, 12989–13001. DOI: 10.1021/ja0473182. (b) Dinolfo, P. H.; Hupp, J. T. Tetra-Rhenium Molecular Rectangles as Organizational Motifs for the Investigation of Ligand-Centered Mixed Valency: Three Examples of Full Delocalization. *J. Am. Chem. Soc.* **2004**, *126*, 16814–16819. DOI: 10.1021/ja045457d.

(44) Crystals featuring other types of strong non-covalent interactions exhibit elastic flexibility: (a) Ghosh, S.; Reddy, C. M. Elastic and Bendable Caffeine Cocrystals: Implications for the Design of Flexible Organic Materials. *Angew. Chem. Int. Ed.* **2012**, *51*, 10319 – 10323. DOI: 10.1002/anie.201204604. (b) Ghosh, S.; Mishra, M. K.; Kadambi, S. B.; Ramamurty, U.; Desiraju, G. R. Designing Elastic Organic Crystals: Highly Flexible Polyhalogenated *N*-Benzylideneanilines. *Angew. Chem. Int. Ed.* **2015**, *54*, 2674 – 2678. DOI: 10.1002/anie.201410730

(45) Similar patterns of alternating strong radical pairing and weaker van der Waals interactions have been observed in supramolecular ring-in-ring assemblies: (a) Lipke, M. C.; Cheng, T.; Wu, Y.; Arslan, H.; Xiao, H.; Wasielewski, M. R.; Goddard, W. A. I.; Stoddart, J. F. Size-Matched Radical Multivalency. *J. Am. Chem. Soc.* **2017**, *139*, 3986–3998. DOI: 10.1021/jacs.6b09892. (b) Cai, K.; Lipke, M. C.; Liu, Z.; Nelson, J.; Cheng, T.; Shi, Y.; Cheng, C.; Shen, D.; Han, J.-M.; Vemuri, S.; Feng, Y.; Stern, C. L.; Goddard, W. A.; Wasielewski, M. R.; Stoddart, J. F. Molecular Russian Dolls. *Nat. Commun.* **2018**, *9*, 5275. DOI: 10.1038/s41467-018-07673-1.

TOC Graphic

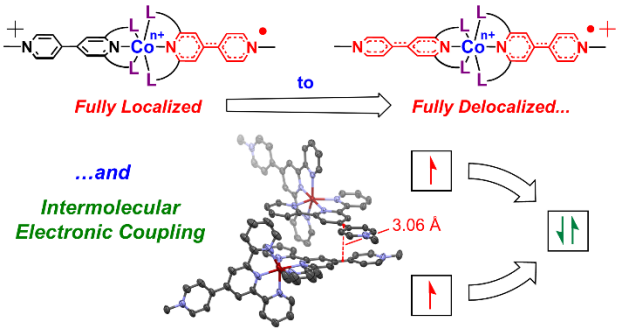
Fully Localized
to
Fully Delocalized...
...and
Intermolecular
Electronic Coupling
3.06 Å